

Journal of Biomedical Optics

SPIEDigitalLibrary.org/jbo

Simultaneous measurement of breathing rate and heart rate using a microbend multimode fiber optic sensor

Zhihao Chen
Doreen Lau
Ju Teng Teo
Soon Huat Ng
Xiufeng Yang
Pin Lin Kei

Simultaneous measurement of breathing rate and heart rate using a microbend multimode fiber optic sensor

Zhihao Chen,^{a,*} Doreen Lau,^b Ju Teng Teo,^a Soon Huat Ng,^a Xiufeng Yang,^a and Pin Lin Kei^b

^aNeural and Biomedical Technology Department, Institute for Infocomm Research, 1 Fusionopolis Way, Connexis, Singapore 138632, Singapore

^bSingapore General Hospital, Department of Diagnostic Radiology, Outram Road, Singapore 169608, Singapore

Abstract. We propose and demonstrate the feasibility of using a highly sensitive microbend multimode fiber optic sensor for simultaneous measurement of breathing rate (BR) and heart rate (HR). The sensing system consists of a transceiver, microbend multimode fiber, and a computer. The transceiver is comprised of an optical transmitter, an optical receiver, and circuits for data communication with the computer via Bluetooth. Comparative experiments conducted between the sensor and predicate commercial physiologic devices showed an accuracy of ± 2 bpm for both BR and HR measurement. Our preliminary study of simultaneous measurement of BR and HR in a clinical trial conducted on 11 healthy subjects during magnetic resonance imaging (MRI) also showed very good agreement with measurements obtained from conventional MR-compatible devices. © 2014 Society of Photo-Optical Instrumentation Engineers (SPIE) [DOI: 10.1117/1.JBO.19.5.057001]

Keywords: breathing rate; heart rate; body movement; ballistocardiogram; noninvasive monitoring; microbend fiber optic sensor.

Paper 140079R received Feb. 8, 2014; revised manuscript received Mar. 31, 2014; accepted for publication Apr. 2, 2014; published online May 1, 2014.

1 Introduction

Simultaneous monitoring of vital signs using noninvasive methods is an important tool in “point-of-care” healthcare sensing. The continuous measurement of cardiopulmonary parameters such as the breathing rate (BR) and heart rate (HR) allows medical professionals to make timely evaluation on the patient’s physiological condition and implement appropriate intervention, in various applications such as telemedicine, critical care, diagnostic imaging, home, and rehabilitative care.

In recent years, there has been a rapid emergence of multiparameter physiologic monitors operating on a noninvasive platform. The new monitors are more comfortable and easy for patient use and enable the automatic measurement of vital signs, without constraint to the person’s activities. These include the Emfit sensor (Emfit Ltd., Kuopio, Finland) and the EarlySense System (EarlySense, Ramat Gan, Israel) monitors. Nevertheless, the use of such electronic sensors are limited in magnetic resonance imaging (MRI), particularly in high-field MRI environment, as they are prone to electromagnetic interference and radiofrequency (RF) heating.¹ There is thus an increasing market demand for safer and effective technical solutions.

The use of optical fiber sensors as physiologic monitors is an attractive option in high-field MRI environment. These optical fibers are intrinsically safe for patient use as they are inert to chemical and are nontoxic. Their dielectric nature and small diameter also allow for their easy installation into miniaturized devices or embedment into medical textiles. In particular, optical fiber sensors are safe for real-time physiologic monitoring during MRI as they are nonferromagnetic, thus immune from electromagnetic and RF interference.

Many of such sensors have been proposed for monitoring of BR, HR, and body movement in the past.²⁻⁹ Grillet et al.²

designed a macrobending sensor that allowed for the monitoring of BR, without simultaneous measurement of BR and HR. The sensitivity of this macrobending sensor is also too low for detection of very weak cardiac-induced vibrations. Hetero-core fiber optic pressure sensors have been proposed for respiration and body movement analysis³ without HR measurement. Fiber Bragg grating (FBG)-based sensors, which have been widely used in structural health monitoring, have recently been proposed for vital signs monitoring. Dziuda et al.^{4,5} illustrated the use of FBG sensors for the simultaneous measurement of BR and HR. However, this wavelength detection-based technology used in the FBG sensors is too complex and expensive for sensor fabrication and instrumentation. A fiber optic statistical mode sensor and a high-order mode excitation sensor have also been proposed for BR and HR measurement.⁶ These sensors nevertheless required highly coherent light source and a bulky high-order mode generator respectively to operate, and no ballistocardiogram (BCG) waveforms were reported. Long-period fiber grating-based sensor and fiber laser have also been used in the monitoring of BR.^{7,8} Although the interferometric fiber optic breathing and HR sensor⁹ has high sensitivity in detection, construction of the sensor system and interrogation is complex and expensive. Last but not least, optical fiber sensing based on plethysmography method for BR and HR measurement has been used only for light transmission, but not for the sensing element.¹⁰

The optical fiber sensor types discussed above may not be the best sensors for industrial acceptance and clinical use due to their bulkiness, design complexity, low-sensor sensitivity, and high-system costs. Homecare monitoring places even more stringent constraints on the system cost, size, noninvasiveness, and ease of use.¹¹ Unfortunately, none of the optical fiber sensor

*Address correspondence to: Zhihao Chen, E-mail: zchen@i2r.a-star.edu.sg

types proposed to date has met these requirements for simultaneous BR and HR measurements. No publication has reported the use of microbend fiber optic sensor for simultaneous BR and HR measurements. We have put great effort these years to reinvent microbend fiber sensors for vital signs monitoring in order to meet the above stringent requirements for home and clinical applications.

In this article, we describe a highly sensitive microbend multimode fiber optic sensor for simultaneous measurement of BR, HR, breathing waveforms, and BCG waveforms. This sensor is noninvasive and is suitable for long-term continuous monitoring of cardiopulmonary parameters with no constraint on the user's activity, and without the need for any prior patient preparation or skin contact.

2 Microbend Multimode Fiber Sensor

2.1 Sensor Design and System Configuration

The working principle behind this sensor is based on the theory of microbending optical fibers, which has been proven both theoretically and experimentally in previous studies.¹²⁻¹⁵ Figure 1 shows the microbend fiber optic sensor system. This system consists of a sensor mat embedded with microbending multimode fiber, a transceiver, and a computer.

The battery-powered transceiver weighs about 100 g and is comprised of a light-emitting diode (LED) light source operating at 1310 nm, a photodetector that is able to detect light signal in the range of 1100 to 1650 nm, amplifiers, simple low-pass filter operating at 250 Hz, an analog-to-digital converter, a microprocessor, and interface circuits for connecting the transceiver to a computer via Bluetooth. The sensor mat was constructed of two microbenders, a section of the multimode fiber, and plastic cover materials as shown in Fig. 2. Figure 3 shows the typical microscope examination of the microbenders (made of polyester fibers).

The optical fiber used for fabrication of the sensor is a standard graded-index multimode fiber with a core diameter of

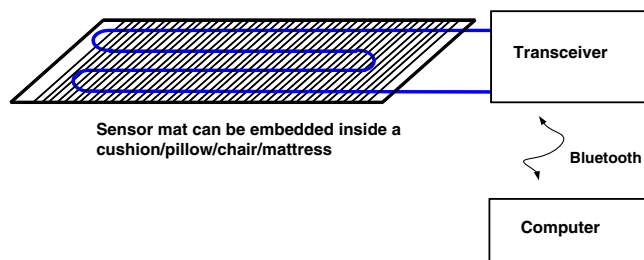


Fig. 1 Microbend fiber sensor system configuration.

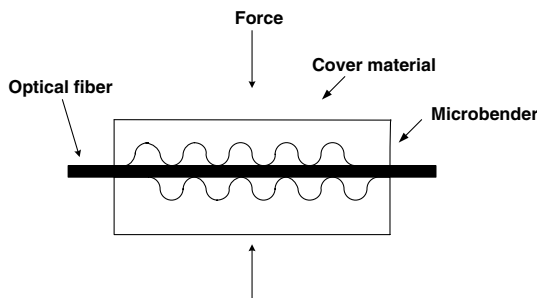


Fig. 2 Design of the microbend fiber optic sensor mat.

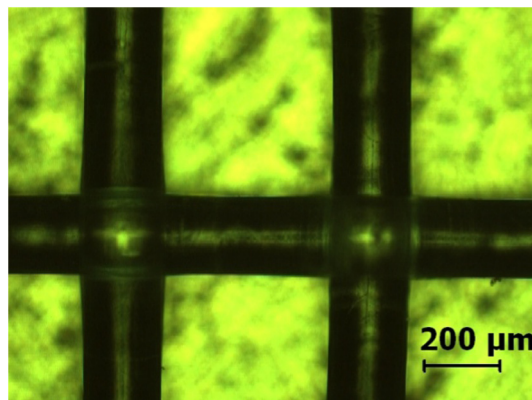


Fig. 3 Microscopic view of a typical microbender.

100 μm and numerical aperture (NA) of 0.272 as the sensing fiber. The mat was constructed to a dimension of 25×20 cm for characterization. The thickness of the sensor mat is < 2 mm and only weighs ~ 65 g, enabling its portability and easily embedment into medical textiles or cushion, pillow, chair, bed, etc. The sensor mat, in response to breathing-induced body movement and heart beating-induced body movement, applies a force ΔF or pressure ΔP to the bent multimode fiber and cause the amplitude of the fiber deformation X to change by an amount ΔX . The transmission coefficient T for light travelling along the bent multimode fiber is changed by an amount ΔT such that¹⁵

$$\Delta T = \left(\frac{\Delta T}{\Delta X} \right) \Delta F \left(k + \frac{AY}{l} \right)^{-1}, \quad (1)$$

where k is the force constant of the bent fiber, A is the cross-sectional area, Y is the Young's modulus, and l is the length of the microbender gap. Detection of the BR, breathing waveform, HR, and BCG was based on modulation in optical transmission. For a high-sensitivity pressure sensor application, Eq. (1) becomes¹⁵

$$\Delta T \cong \frac{\Delta T}{\Delta X} A_p k^{-1} \Delta P, \quad (2)$$

where A_p is the area of the deformer and ΔP is the change in pressure. Maximum microbend sensitivity is achieved by proper construction of the optical fiber such that the spatial frequency Λ of the microbenders for graded-index multimode fiber satisfies the follow approximate relationship¹⁵

$$\Lambda = \frac{2\pi \cdot a \cdot n_0}{\text{NA}}, \quad (3)$$

where a is the fiber core radius, n_0 is the refractive index of the core, and NA is the numerical aperture of the fiber. Equation (3) applies to graded-index multimode fiber. Step-index multimode fiber can also be used for fabrication of sensor mat. In this case, the spatial frequency Λ of the microbenders is given by¹⁵

$$\Lambda = \frac{\sqrt{2}\pi \cdot a \cdot n_0}{\text{NA}}. \quad (4)$$

The microbending loss occurs as the guided modes are coupled to radiation modes. Effective coupling between the

guided modes and radiation modes can be achieved with the spatial frequency Λ given by Eqs. (3) and (4) for graded-index and step-index multimode fibers, respectively. However, graded-index fibers are better than step-index fibers because graded-index fibers have resonance condition, where the microbending loss is sharply peaked while step-index fibers do not have the resonance condition.¹² So, we choose graded-index multimode fibers for our sensor mat in this article.

The graded-index multimode fiber we used is glass optical fibers. One potential problem with using glass optical fibers is that there is a risk to the users or patients when glass optical fibers break. The pieces of the glass optical fiber may puncture skin causing bodily injury. This is not acceptable in the application. Patient's safety is the first priority. Another problem was that glass optical fibers can be easily broken. In biomedical applications, plastic optical fibers are preferred because plastic optical fibers are biocompatible. More importantly they are more rugged and enable greater safety than glass optical fibers. In this article, however, we use glass graded-index multimode fiber for proof of concept demonstration only. In product manufacturing, the use of plastic optical fibers is preferred.

The sensor design is based on microbending effect created through a "sandwich" microbender structure as shown in Fig. 2. Under mechanical perturbation ΔF such as periodic body movements induced by breathing and cardiac biomechanical forces, the microbenders squeeze the multimode fiber and induce a series of microbends along the fiber axis. Microbending causes light coupling from core-guided modes into radiation modes, resulting in irreversible light loss and modulation in the light intensity detected by the photodetector inside the transceiver. By extracting the modulated light intensity, the BR, breathing waveforms, HR, BCG waveforms of the patient, and other body movement information within a specific time can be processed and measured using the digital signal processing (DSP) algorithm we have developed. The electrical output of the transceiver was wirelessly connected to a computer via Bluetooth sampled at a rate of 50 Hz. There was no crosstalk between this frequency and the grid frequency in the lab and hospital environment in Singapore. It is easy to change the sampling rate to other sampling rate whenever needed.

2.2 Key DSP Algorithms

Figure 4 shows the general workflow in processing a measured signal using the algorithm. Smoothing and filtering are applied after receiving raw data from the transceiver followed by data quality check and peak detection in the time domain for calculation of the BR and HR. The final BR, breathing waveforms, HR, BCG waveforms were then displayed on the graphical user interface (GUI). LabVIEW (National Instruments Corporation, Austin, Texas) programming language was used to design this application software.

Below are more detailed descriptions on the algorithms used for extraction of breathing component and heart-beating component from measured signals and for noise suppression.

2.2.1 Breathing component extraction

Due to the relatively high-sampling rate for heart beat signal acquisition, large amount of averaging is needed for smoothing for robust analysis and calculation of the BR. These comprise of three stages of curve-smoothing by using averaging filters to remove unwanted high-frequency spikes so that the breathing

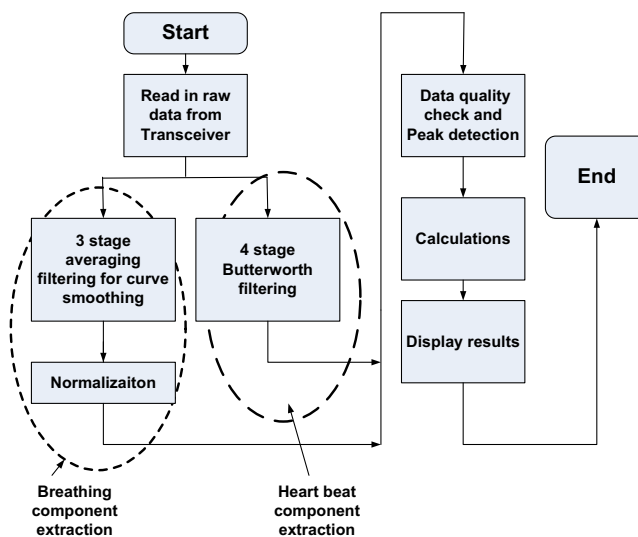


Fig. 4 Workflow in processing a measured signal using the algorithm.

waveform can be recovered. This is followed by normalization to the reference level of zero to remove direct current (DC) drift and fluctuation caused by external noises. After which, the peak locations will be detected by the "peak-detector" module. Upon detecting the peak locations, the respiratory period can be found for calculation of the BR.

2.2.2 Heart beat component extraction

Although the heart-beating signal is very weak as compared to the breathing signal, the heart-beat signal can still be easily extracted because the frequency bands of breathing and heart beat signals are well separated. For example, breathing frequencies for adults are located between 0.05 and 0.6 Hz at rest, whereas heart beat frequencies are occur between 0.8 and 2.0 Hz. Based on these features, a filter method was used to remove breathing signal and suppress other noises. We found that the Butterworth filter is a suitable filter. Butterworth filters were applied to the raw data to obtain BCG waveforms within the frequency range from 0.8 to 25 Hz. After which, the heart beat locations were detected by the "peak-detector" module. After locating the heart beat pulses, the heart beating period can be obtained.

2.2.3 Noise suppression

In the data quality check, level threshold algorithms are applied. When there is a large change of amplitude from large body movement noise, such as change of body position (threshold value of 1500 in our case) as compared with the amplitude from 600-effective point averaging, peak detections for both BCG and respiratory waveforms will ceased until the movement-caused large fluctuation has stopped. At the same time, the movement count will be registered. When the amplitude of the filtered BCG waveform is more than 200 (peak-to-peak), which may result from actions such as talking, etc, detection will stop temporary as a typical amplitude of a filtered BCG waveform is 80 (peak-to-peak). Movement count will not be registered in this case. This level threshold for the BCG waveform is used to suppress small spurious body movement noises.

According to the frequency feature of heart beating, it is obvious that irregular breathing patterns have little effect on the heart-beat rate measurement because the frequency band

of either regular breathing patterns or irregular breathing patterns, do not coincide with the frequency band of heart beat signals. Hence, interference from breathing signal noise is negligible. It should be noted that breathing action has an effect on HR variability measurement via the phenomenon of respiratory sinus arrhythmia (RSA).¹⁶ We do observe the shortening of the J-J interval component of the BCG waveform during inspiration and prolonged J-J interval during expiration. This means that our current algorithm is able to pick up beat to beat information of heart beat signal.

2.3 Sensor Characteristics

The proposed design of the microbend sensor is shown in Fig. 2. A graded-index multimode fiber with a core diameter of 100 μm and NA of 0.272 was used as the sensing fiber for construction of this sensor. The mat was constructed to a dimension of 25 × 20 cm. Figure 5 shows a typical plot of sensor output *P* as a function of weight *F*, where the optical signals have been converted into electrical signals. The force is applied uniformly over the area of 0.05 m² within the sensor mat. This is a typical microbend sensor response characteristics similar to the results shown in Ref. 17. The key difference in the sensor response with the load is that the output of our microbend fiber sensor decreases slower than the sensors in Ref. 17. Our experimental data fits a Gauss curve perfectly, in which

$$P = P_0 + \frac{B}{w\sqrt{\pi/2}} \exp\left[-2\frac{(F - F_0)^2}{w^2}\right], \quad (5)$$

where $P_0 = 0.00251$, $B = 8.34117$, $w = 12.681$, $F_0 = -2.58835$. From Eq. (5), the sensor sensitivity *S* can be calculated as

$$S = \left| \frac{dP}{dF} \right| = \frac{4B(F - F_0)}{\sqrt{\pi/2}w^3} \exp\left[-2\frac{(F - F_0)^2}{w^2}\right]. \quad (6)$$

Figure 6 shows the sensor sensitivity curve as a function of weight based on the fitting data according to Eq. (6). For this specific sensor design, there are three distinct regions of sensitivity. The first region is the nonlinear region from 0 to 3.7 kg and the sensor sensitivity hits peak of 0.05 V/kg at about

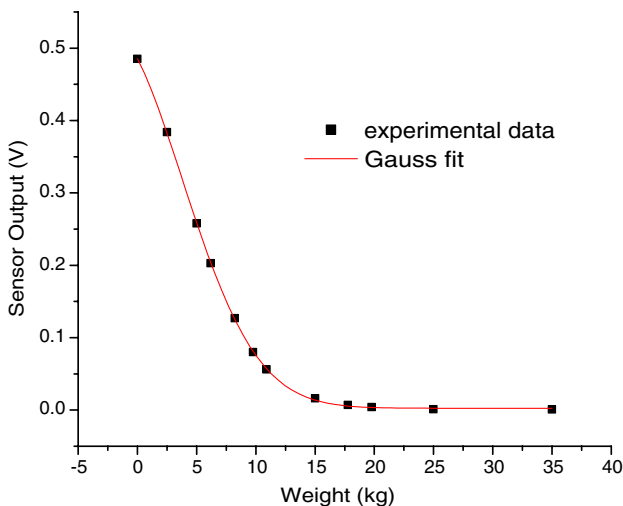


Fig. 5 Sensor output as a function of weight of the sensor mat.

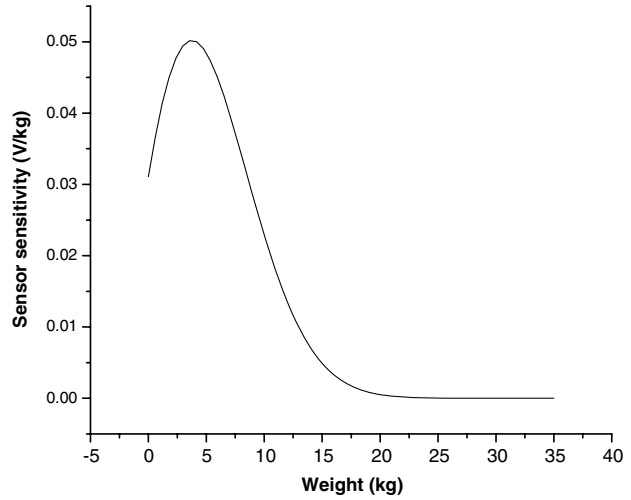


Fig. 6 Sensor sensitivity as a function of weight of the sensor mat.

3.7 kg. The second region is the approximately linear region from 3.7 to 15 kg wherein the sensor sensitivity decreases. The third region is from 15 to 17 kg and then becomes zero after 17 kg. This zero sensitivity results mainly from no signals detected by the detector due to large optical loss induced. The force sensitivity of current design is good enough for detection of very weak signals, e.g., changes in cardiac force due to heart beating. No excessive bending is needed for low values of load.

2.4 Sensor Optimization for Various Applications

To avoid zero force sensitivity and to extend the working range of the sensor mat so as to cater for various body weights for various applications as shown in Fig. 7, sensor designs can be optimized to handle different ranges of applied force. Key design parameters are core diameter and NA of the multimode fiber as well as spatial frequency of mechanical perturbation along the fiber axis. The sensor performance shown in Figs. 5 and 6 is good for bed application in the lying position. The sensor mat is placed under the upper thoracic region (head-shoulder area) of the monitored subject. In this case, only part of the body weight is applied to the sensor mat. It should be noted that if the sensor mat is placed under a mattress with a 7-inch thickness, e.g., heart beat signal cannot be detected using current sensor mat whereas breathing signal is still detectable. This means that a very thick mattress placed in between our sensor mat and the subject can considerably obstruct the propagation of body vibrations by heart beating to the sensor mat, as our sensor requires body contact for measurement of biomechanical signals.

As for seating and standing application, significant body weight is applied to sensor mat. As can be seen from Figs. 5 and 6, the relationship between sensor output and applied force is not linear. The dynamic working range is <13 kg in this case. To overcome this problem, we propose a “spacer technique” to extend the working range of the sensor mat. A dummy plastic tube is used as a spacer to lessen the impact of the applied force to the fiber so as to increase the sensor mat’s dynamic working range. The spacer is located with the sensing multimode fiber in between microbenders. Figure 8 shows the sensor output as a function of weight. It can be seen from Fig. 8 that with the spacer, the sensor’s dynamic range of operation is extended beyond 100 kg while the sensor could not work



Fig. 7 Various applications of sensor mats: bed, pillow, chair, and standing application.

beyond 15 kg without the spacer despite using the same fiber. Another simple way to extend the working range of the sensor mat so as to cater for large applied force is to use 50- or 62.5- μm multimode fiber instead of 100- μm multimode fiber for given microbenders. We have demonstrated that a sensor mat made of 62.5- μm multimode fiber is good for the seating application.

A sensor mat with an area of 0.05 m² was built for standing application (see the first photo from right in Fig. 7). In this application, the whole body weight is applied to the sensor mat. This sensor mat uses 62.5- μm multimode fiber. Figure 9 shows BCG waveform (acquired over a period of 6 s) in the standing application. Only the HR can be measured for this standing application using our current DSP algorithm. The impact to the sensor mat from breathing-induced body vibration is so weak that BR cannot be measured using our current algorithm. However, BR may be derived based on breathing-induced modulation on the BCG according to the phenomenon of RSA. We are currently in

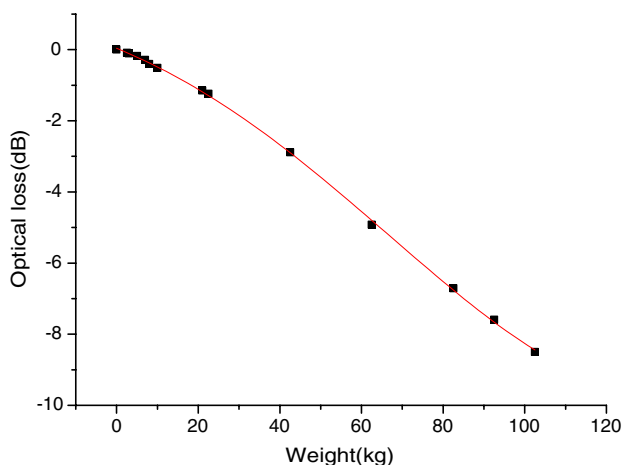


Fig. 8 Sensor output as a function of weight.

the process of developing a new DSP algorithm for BR measurement for the standing application.

3 Measurement Results and Discussions

The prototype system of our sensor mat and transceiver is shown in Fig. 10. According to the system setup shown in Fig. 1, the typical amplitude induced by breathing is about 800 (after digitalization), and the cardiac force-induced amplitude is about 70 as shown in Fig. 11. This showed the capability of our sensor in detecting breathing-induced body movement and even weak vibrations or changes in cardiac force.

Figure 12 illustrates the GUI of the application software. It displays the HR, BCG waveform, BR, breathing waveform, number of large body movement, and number of apnea events. The display is user-friendly and contains an alarm system to alert the medical staff of adverse events.

Figure 13 shows the typical BCG waveform of a healthy subject according to Ref. 11, in which the main components of a BCG waveform consist of H, I, J, K, L, and N waves. Figure 14 is a BCG signal obtained from a healthy subject in our study. The features of this waveform closely resemble the BCG waveform shown in Fig. 13 although two different techniques were used. These BCG features may potentially be used for diagnosis of heart disease.

It is interesting to know how much force is exerted on the sensor mat due to breathing and heart beating actions. To do so, we used a sensor mat with an area of 0.05 m² built for standing application above for the measurement of heart beating-induced force. The following method is used for estimation of the heart beating-induced force.

3.1 Calibration Phase

In this phase, body weight, W_b , is not applied to the sensor mat. Data is acquired in the preset period of 20 s. The mean of the curve, W_c , is calculated.



Fig. 9 A 6-s acquisition of ballistocardiogram (BCG) waveform from a healthy subject in the standing position.



Fig. 10 Prototype system of the microbend fiber optic sensor mat and transceiver.

3.2 Measurement Phase

In this phase, body weight is applied to the sensor mat. Data is acquired in the preset period of 20 s. The mean of the curve, W_m , is calculated. At the same time, arithmetic mean of the IJ and JK amplitude, W_{ijk} , is calculated.

3.3 Estimation of Heart Beating Induced Force

In this phase, the heart beating-induced force, $F = W_b / (W_c - W_m) * W_{ijk}$. We have estimated the heart beating-induced force of two subjects using this method. The heart beating-induced force of a 51-year-old man and a 32-year-old man

are 0.18 and 0.3 kg, respectively. A similar measurement method is applied for breathing-induced force measurement. As the acquisition of breathing signal is indirect in the standing position, we chose the seating position for the measurement. The breathing-induced force applied to the sensor mat is about 1 to 2 kg depending on shallow and deep breathings.

The local maxima in breathing and BCG waveforms showed in Fig. 12 are used for BR and HR calculation. The BR and HR are defined as

$$\text{BR} = \frac{60}{T_n - T_{n-1}}, \quad (7)$$

$$\text{HR} = \frac{60}{t_n - t_{n-1}}, \quad (8)$$

where T_n is the time at n 'th local maxima and T_{n-1} is the time at $(n-1)$ 'th local maxima in the breathing waveform, t_n is the time at n 'th local maxima and t_{n-1} is the time at $(n-1)$ 'th local maxima in the BCG waveform. BR and HR are expressed in beats per minute (bpm). This article is not aimed for beat to beat measurement although our sensor has the capability to do it as shown in Fig. 12. In our present study, we focus only on simultaneous measurement of BR and HR within a specific period of time.

Table 1 shows the simultaneous measurement of the BR and HR from a 32-year-old healthy male subject (body weight: 65 kg) using our microbend sensor. The sensor mat was placed on top of a mattress and under a very thick bed sheet. The subject was asked to lie still (see the second photo from the left in Fig. 7). Measurements were recorded within 1 min (measurement every 6 s) and compared with a commercial physiologic monitoring device (BioHarness™, Zephyr Technology Corporation, Maryland) and a SpO₂ device (OxyWatch™ Finger Pulse Oximeter). The maximum error detected was only ± 2 beats per minute (bpm) for both BR and HR measurements.

In the second experiment, the second subject is a healthy male of age, 28-year-old and weight 70 kg. Figure 15 shows BR and HR plots of the subject acquired using our sensor mat and a commercial device, Zephyr sensor. Zephyr sensor is a wearable sensor, which can be worn on the chest for BR and HR measurements. Key experimental results are

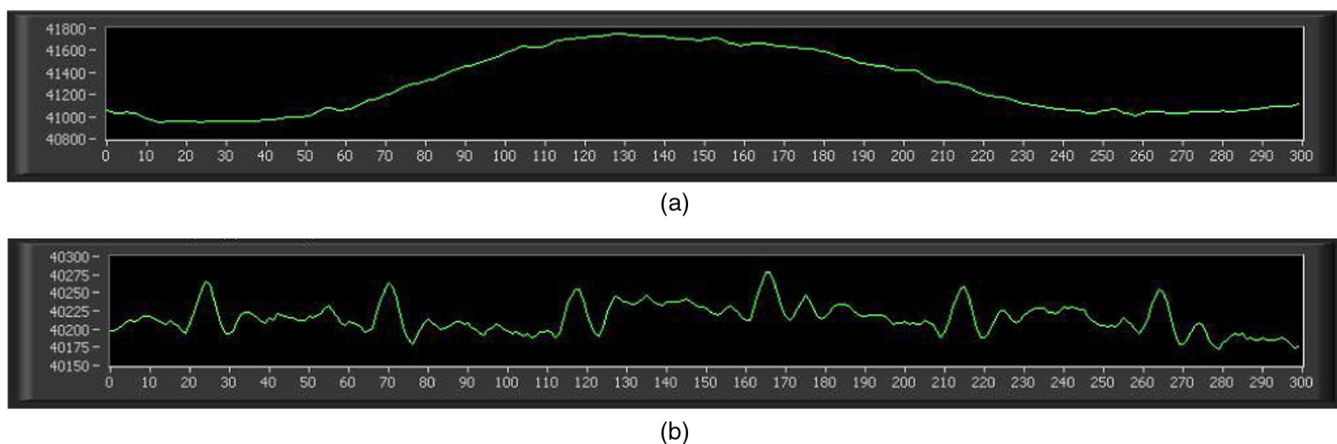


Fig. 11 (a) Sensor output after digitalization: Breathing induced body movement. (b) Sensor output after digitalization: Cardiac force induced body movement.

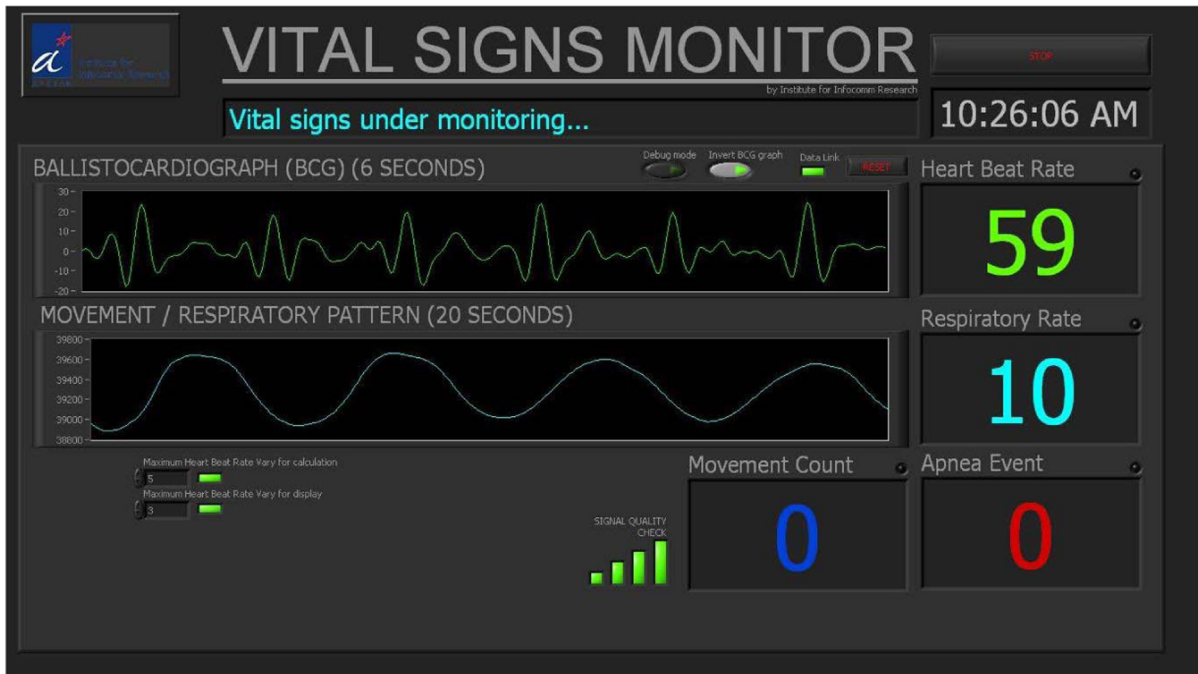


Fig. 12 User display of the application software.

summarized in Table 2. The recording time is 3495 s. Our sensor recorded 10 samples each second, while the Zephyr sensor recorded one sample for each second. The mean values of BR measured from both sensors are comparable. The absolute error of the BR mean values is <2 bpm and the relative error is 9.7%. An accuracy of ± 2 bpm for the BR measurement should be acceptable for monitoring physiologic application. As for HR measurement, the mean values of HR measured from the two sensors are quite similar; the absolute error for HR mean values is <0.5 bpm and the relative error is $<1\%$. The standard deviations for BR measurements are small, 0.95 bpm for Zephyr sensor and 1.38 bpm for our sensor mat, respectively. The standard deviations for HR measurement are about 3 bpm for both our fiber optic sensor and the reference Zephyr sensor. As can be seen in Fig. 15, our sensor and Zephyr sensor have different waveform shapes for BR. This is because our sensor takes a longer time or more number of local maxima for BR calculation. Zephyr sensor is aimed for sports application and warranted

short time or less number of local maxima for BR calculation. However, in HR measurement, both our sensor and Zephyr sensor have similar waveform shapes. We have used four local maxima for HR calculation using our fiber optic sensor. It is not justified to calculate the “real time” difference between measured values from our sensor and Zephyr sensor because both sensor systems use different algorithms and average time for BR and HR calculations although we have synchronized both devices for recording. We have observed that there is a delay in displaying the same results between two sensors.

Zephyr sensor is a device that requires direct body skin contact for physiologic monitoring, thus has less motion noise issues. Our sensor does not require direct skin contact, i.e., it can be embedded in bed and chair, etc. Thus, our sensor is very sensitive to motion noises. For example, the other body movement, such as changes in body position, can distort both the breathing waveform and the BCG waveform. Even very small body movements like muscle tremor, swallowing,

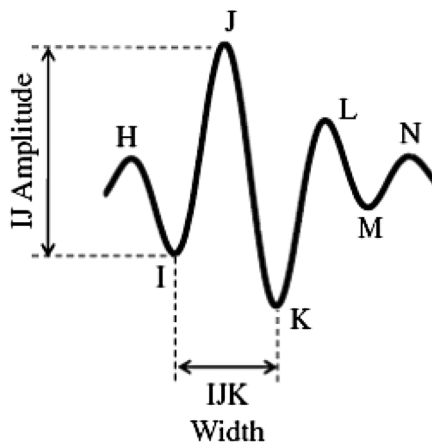


Fig. 13 BCG signal obtained from a healthy subject.¹¹

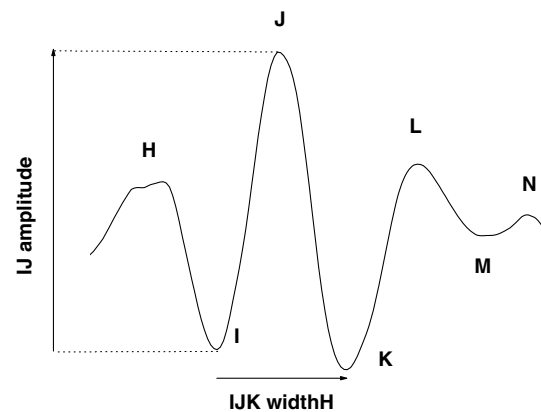


Fig. 14 BCG signal obtained from a healthy subject in this study using our microbend fiber optic sensor system.¹⁸

Table 1 Experimental results comparing the breathing rate (BR) and heart rate (HR) measurements obtained from a healthy male subject within 1 min using our microbend sensor with commercial physiologic monitoring devices.

Microbend sensor		Zephyr sensor		OxyWatch SpO ₂	
BR (bpm)	HR (bpm)	BR (bpm)	HR (bpm)	BR (bpm)	Pulse (bpm)
6	79	7	81	NA	80
6	80	7	78	NA	78
8	81	8	79	NA	79
10	83	10	82	NA	84
10	79	11	79	NA	79
14	80	14	80	NA	79
12	77	14	76	NA	76
10	79	11	79	NA	78
12	82	11	83	NA	82
14	78	12	78	NA	79

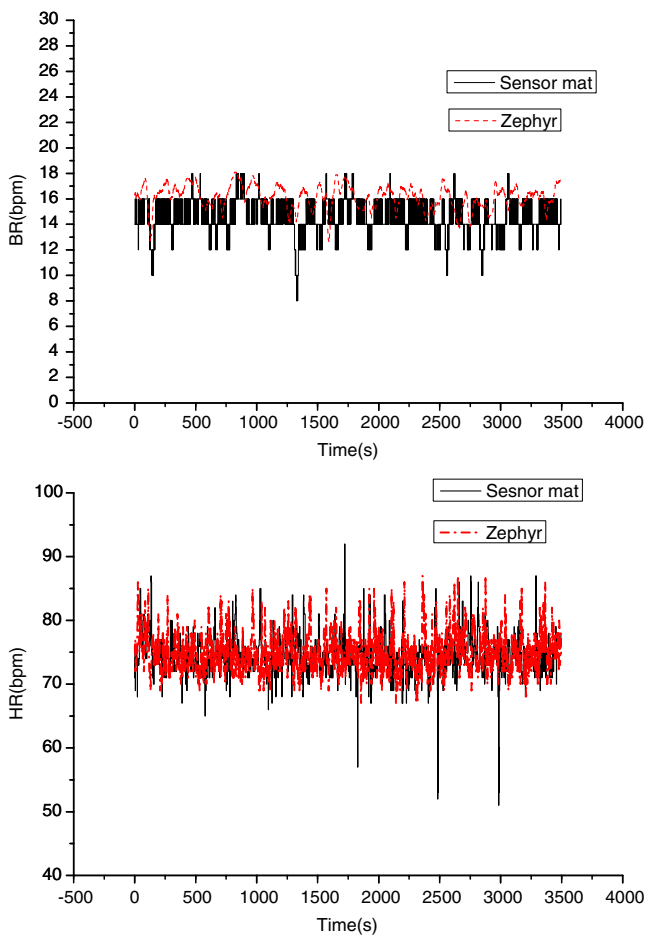


Fig. 15 Breathing rate (BR) and heart rate (HR) curves obtained from a healthy subject at rest in this study using our microbend fiber optic sensor system and Zephyr sensor.

Table 2 Summary of the experimental results for the second experiment.

	Sensor type		Error	
	Zephyr sensor	Our sensor mat	Absolute error	Relative error
Recording time (s)	3495	3495		
Breathing rate				
Mean BR (bpm)	16.14	14.57	1.57	9.7%
SD (bpm)	0.95	1.38		
No. of samples	3495	34951		
Heart rate				
Mean HR (bpm)	74.98	74.49	0.49	0.7%
SD (bpm)	3.06	3.07		
No. of samples	3495	34951		

etc. can also distort the BCG waveform. Although we have applied the algorithm for motion noise removal, we can still see the spikes in our results as shown in Fig. 15. Fortunately, these spike amplitudes are very high and their duration is short. These spikes did not affect our final results and simultaneous measurement of BR and HR.

We did the same experiment on another day. The results for the third experiment are shown in Table 3. Similar results were found.

We have also performed a preliminary clinical trial in the 3.0 Tesla (T) MRI environment to compare the performance of our microbend fiber optic sensor with conventional MR-compatible monitoring system (Respiratory bellows and Pulse Oximeter, Physiological Measurement Unit, Siemens Medical Solutions,

Table 3 Summary of the experimental results for the third experiment.

	Sensor type		Error	
	Zephyr sensor	Our sensor mat	Absolute error	Relative error
Recording time (s)	3435	3435		
Breathing rate				
Mean BR (bpm)	16.68	15.03	1.65	9.9%
SD (bpm)	1.03	1.35		
No. of samples	3435	34350		
Heart rate				
Mean HR (bpm)	72.58	72.24	0.34	0.5%
SD (bpm)	3.2	2.9		
No. of samples	3435	34350		

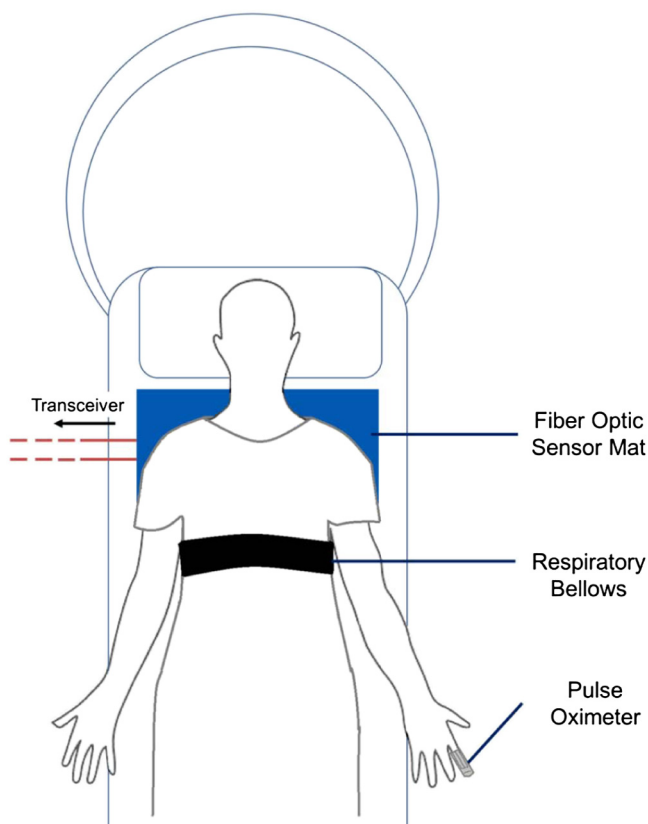


Fig. 16 Experimental setup of the microbend fiber optic sensor mat in the magnetic resonance imaging (MRI) room. The sensor mat was placed under the thoracic region of all trial subjects for simultaneous monitoring of the BR and HR during liver MRI scan. Measurements obtained at every 5-min intervals were compared with conventional respiratory bellows (for the BR) and finger pulse oximeter (for the pulse rate).

Erlangen, Germany) (Fig. 16). The experiment was conducted during the MRI liver scans of 11 nonanesthetized healthy subjects of ages 26 to 62-years old (6 males and 5 females). The body weights of these subjects were in the range 46.6 to 80.0 kg (mean 60.3 kg). In this clinical trial, we were not allowed to interface with any MRI machine and devices. So, we had to manually record our experimental results. Our results demonstrated good agreement in simultaneous BR and HR measurements between our microbend sensor and the conventional physiologic monitoring system (Table 4, Figs. 17 and 18). Figure 19 shows the axial and coronal images obtained during

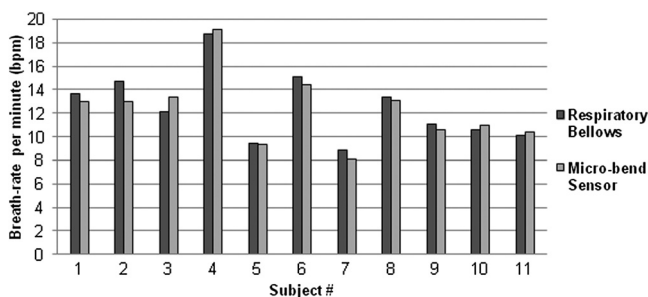


Fig. 17 BR detected and recorded for all 11 healthy subjects by each respiratory monitoring device during MRI showed maximum error of ± 1.7 bpm (standard deviation is 0.5 bpm).

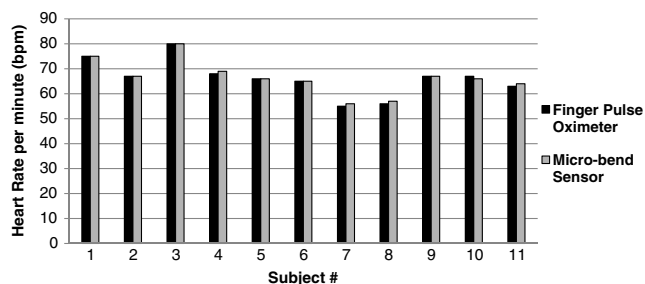


Fig. 18 HR detected and recorded for all 11 healthy subjects by each HR monitoring device during MRI showed maximum error of ± 1.2 bpm (standard deviation is 0.4 bpm).

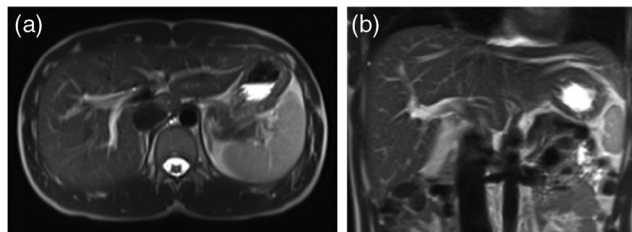


Fig. 19 (a) and (b) the axial and coronal images obtained during MRI liver scan of a healthy subject under physiologic monitoring using our microbend optical fiber sensor. No image distortion or radiofrequency artifacts were seen in all images obtained from the trial subjects, despite the presence of the sensor mat inside the MRI gantry, suggesting the MR-compatibility of the sensor.

Table 4 A good agreement between our microbend sensor and conventional MR-compatible devices in the mean measurements of the BR and HR recorded for every 5-min interval during a 30-min MRI scan session on 11 clinical trial subjects.

BR monitoring			
Device	Respiratory bellows	Microbend sensor	Pearson correlation
BR (bpm)	12.53 \pm 2.94	12.31 \pm 2.97	$r = 0.963$; $p = 0.000 < 0.001$
HR monitoring			
Device	Finger pulse oximeter	Microbend sensor	Pearson correlation
HR (bpm)	66.27 \pm 7.17	66.55 \pm 6.86	$r = 0.997$; $p = 0.000 < 0.001$

MRI liver scan of a healthy subject under physiologic monitoring using our sensor. An examination and evaluation of all MR images obtained during physiologic monitoring using our microbend sensor and hospital equipment were conducted by using the same method presented in Ref. 19. They were quantitatively evaluated for the liver signal-to-noise ratio and liver-to-spleen contrast-to-noise ratio. In addition, MR image quality was qualitatively analyzed based on the five-point image scoring scale. Results showed no obvious image distortion and RF artifacts in the clinical report. This study suggested the feasibility in using our sensor mat for physiologic monitoring during MRI. Our sensor was able to detect a comparable BR and HR to the predicate devices and produce liver MRI images of good and comparable image quality to the prospective acquisition correction technique navigator-acquired scans in 3.0-T MRI environment.

As demonstrated in this article, our device works very well for normal subjects. As for abnormal breathing and heart beating cases, we believe our device can still apply. The key is that our sensor can recover correct breathing waveform and BCG waveform. We clearly observed the phenomenon of RSA, where BCG J-J interval was shortened during inspiration and prolonged during expiration. Peak detection in the algorithm is independent of regular or irregular beat-beat intervals. This shows our device can be potentially used for abnormal breathing and heart beating subjects.

4 Conclusions

We have presented a highly sensitive microbend fiber sensor for simultaneous measurements of BR and HR. Comparative testing between our microbend fiber optic sensor and commercial physiologic sensors showed comparable and good agreement in simultaneous measurements of BR and HR, with an accuracy of ± 2 bpm. The measured BCG waveforms closely resemble BCG waveforms described in the existing literature. Furthermore, our preliminary trial on 11 healthy human subjects during MRI also showed very good agreement in BR and HR measurements obtained between our microbend fiber optic sensor and conventional MR-compatible monitors. Although the subject size for the testing in this article is small, our sensor demonstrated the feasibility for simultaneous measurements of BR and HR in a nonbody skin contact way. The proposed sensor system is MR-safe and has the potential to replace conventional MR-compatible physiologic devices for cardiopulmonary condition monitoring and possible physiologic motion-gating function during MRI. The sensor design is simple and requires low-fabrication cost, which may facilitate industrial acceptance and commercialization for use in various hospital settings and even at home.

Acknowledgments

This work was funded by the Agency for Science, Technology and Research (A*STAR) Biomedical Engineering Program and A*STAR-MINDEF Joint Program. The authors would like to thank all reviewers' comments.

References

1. B. A. Holshouser, D. B. Hinshaw, and F. G. Shellock, "Sedation, anesthesia and physiologic monitoring during MR imaging: evaluation of procedures and equipment," *J. Magn. Reson. Imaging* **3**, 553–558 (1993).
2. A. Grillet et al., "Optical fibre sensors embedded into medical textiles for healthcare monitoring," *IEEE Sensors J.* **8**(7), 1215–1222 (2008).
3. M. Nishiyama, M. Miyamoto, and K. Watanabe, "Respiration and body movement analysis during sleep in bed using hetero-core fiber optic pressure sensors without constraint to human activity," *J. Biomed. Opt.* **16**(1), 017002 (2011).
4. L. Dziuda et al., "Monitoring respiration and cardiac activity using fiber Bragg grating-based sensor," *IEEE Trans. Biomed. Eng.* **59**(7), 1934–1942 (2012).
5. L. Dziuda et al., "Fiber Bragg grating based sensor for monitoring respiration and heart activity during magnetic resonance imaging examinations," *J. Biomed. Opt.* **18**(5), 057006 (2013).
6. W. B. Spillman et al., "A smart bed for non-intrusive monitoring of patient physiological factors," *Meas. Sci. Technol.* **15**, 1614–1620 (2004).
7. T. Allsop et al., "Application of long period grating sensors to respiratory function monitoring," *Proc. SPIE* **5588**, 148–156 (2004).
8. J. Wo et al., "Noninvasive respiration movement sensor based on distributed Bragg reflector fiber laser with beat frequency interrogation," *J. Biomed. Opt.* **19**(1), 017003 (2014).
9. S. Spranger and D. Zazula, "Detection of heartbeat and respiration from optical interferometric signal by using wavelet transform," *Comput. Methods Prog. Biomed.* **111**, 41–51 (2013).
10. L. G. Lindberg, H. Ugnell, and P. A. Oberg, "Monitoring of respiratory and heart rates using a fibre-optic sensor," *Med. Biol. Eng. Comput.* **30**, 533–537 (1992).
11. T. Inan et al., "Robust ballistocardiogram acquisition for home monitoring," *Physiol. Meas.* **30**, 169–185 (2009).
12. J. W. Berthold, "Historical review of microbend fibre-optic sensors," *J. Lightwave Technol.* **13**, 1193 (1995).
13. S. T. Lee et al., "A microbend fibre optic pH sensor," *Opt. Commun.* **205**, 253–256 (2002).
14. M. Linec and D. Donlagic, "A plastic optical fiber microbend sensor used as low cost anti-squeeze detector," *IEEE Sensors J.* **7**, 1262–1267 (2007).
15. N. Lagakos, J. H. Cole, and J. A. Bucaro, "Microbend fiber-optic sensor," *Appl. Opt.* **26**, 2171–2180 (1987).
16. M. Moser et al., "Phase- and frequency coordination of cardiac and respiratory function," *Biol. Rhythm Res.* **26**(1), 100–111 (1995).
17. D. Donlagic and B. Culshaw, "Microbend sensor structure for use in distributed and quasi-distributed sensor systems based on selective launching and filtering of the modes in graded index multimode fiber," *J. Lightwave Technol.* **17**(10), 1856–1868 (1999).
18. Z. Chen et al., "Portable fiber optic ballistocardiogram sensor for home use," *Proc. SPIE* **8218**, 82180X (2012).
19. D. Lau et al., "Intensity-modulated microbend fiber optic sensor for respiratory monitoring and gating during MRI," *IEEE Trans. Biomed. Eng.* **60**(9), 2655–2662 (2013).

Zhihao Chen is a senior scientist with the Neural and Biomedical Technology Department at A*STAR Institute for Infocomm Research, Singapore. He is the principal investigator and project manager of various research projects and industrial projects on sensors for various applications. His research interests include optical fiber sensors, optical and electrical sensors for biomedical applications and industrial applications. He and his team reinvented the microbend fiber sensor for vital signs monitoring for hospital and home use.

Doreen Lau was a research assistant at Department of Diagnostic Radiology, Singapore General Hospital. She received her BSc in life sciences from the National University of Singapore and Specialist Diploma in Biomedical Engineering from Singapore Polytechnic in 2009 and 2014, respectively. She has a diverse research background in medicine, biology and medical engineering. She specializes in bioimaging and molecular genetics research on animal models, and has experience in medical imaging and fiber optic sensors research on humans.

Ju Teng Teo received the BEng (EEE) degree, in 2008, and the MSc (Elec) degree, in 2010, from Nanyang Technological University, Singapore. He is presently with Institute for Infocomm Research, as a research engineer. His main research interest includes developing optical fiber sensors and algorithms for vital signs monitoring. He

has developed various sensors and customized software for field trials in hospitals.

Soon Huat Ng is a research engineer in the Neural & Biomedical Technology Department at the Institute for Infocomm Research. He received his BEng degree in electrical and electronic engineering from Nanyang Technological University in 2007. His main research interests include the development and application of novel methods for patient vital signs monitoring.

Xiufeng Yang is a research scientist at the Institute for Infocomm Research, Singapore. She received her ME degree and PhD degree in communication and optics from Tianjin University and Nankai

University China in 1994 and 1998, respectively. Her research interests are fiber optic based devices and sensors. She has been working on fiber sensor based vital signs monitoring and fiber laser and interferometry based vibration monitoring.

Pin Lin Kei is a radiologist and clinical principal investigator at Department of Diagnostic Radiology, Singapore General Hospital. He received his medical degree from the University of Glasgow, UK, in 2001, Master of Medicine (diagnostic radiology) in 2006 from Singapore, and FRCR (UK) in 2006. He specializes in advanced medical imaging techniques such as CT and MRI, and has special interest in biomedical optics research.